JOURNAL OF GEOPHYSICAL RESEARCH, VOL. 87, PAGES 3481-3488, MAY 1, 1982

THE HIDDEN ION POPULATION OF THE MAGNETOSPHERE

Richard C. Olsen

Physics Department, The University of Alabama in Huntsville
Huntsville, Alabama, 35899

Abstract. Particle data from two geosynchronous satellites (Applied Technology Satellite 6 and SCATHA) show a normally hidden ion population appearing when the satellites are in the earth's shadow. Ion and electron data show the spacecraft potential dropping from +10 V in sunlight to +4 to +5 V in eclipse at local midnight, in low-energy (T < 1 keV) plasma sheet environments. During eclipse, a cold (T = 1 eV), dense (n = 10-100 cm^{-3}), isotropic ion population appears which was invisible in sunlight because of the larger positive spacecraft potential. Higher-energy populations generally cover the tails of the hidden ion populations, so they cannot be inferred from daylight data. The isotropic population appears only in a few percent of the spacecraft eclipse events, appearing only at times of low K_p (2 or less, preceded by a day with $\Sigma K_p < 20$). A low-energy (T = 1-2 eV) field-aligned population often appears with and without the isotropic population, at slightly higher flux levels. These fluxes are visible in sunlight, but again the distribution functions obtained in eclipse differ from those that would be inferred from daylight data. Measurement of the thermal plasma population on a consistent basis, particularly in the plasma sheet, will require some method of controlling the detector potential with respect to the ambient plasma.

Introduction

Observations of the plasma population of the magnetosphere by particle detectors made over the past two decades have generally left open the question of how completely the plasma population is being measured. In particular, the thermal (0-100 eV) population can be missed because of nonzero spacecraft potentials. Comparisons to absolute measurements in the plasmasphere and plasma sheet have been made in a few cases. Gurnett and Frank [1974] compared 50-eV to 38-keV plasma measurements in the plasma sheet to the total electron density determined from the local plasma frequency and found good agreement in most regions, though there were some discrepancies. These discrepancies were attributed to an unmeasured thermal plasma population which was contributing up to 50% of the total ion density.

Decreau et al. [1978] compared plasma density measurements from six different experiments on the CEOS 1 satellite. Densities were determined between L = 3 and L = 7, along with the spacecraft potential and plasma temperatures. The wave and particle detectors agreed with each other as long as the satellite was in the plasma-sphere and negatively charged. Once the satellite moved into the plasma sheet and began to charge positively, the ion detectors began to report substantially lower plasma densities than the other instruments, even with corrections for the potential. It is possible that the particle detectors were missing a higher-energy (key') population or a field-aligned component of the plasma. A third possibility is that a cold ion population was excluded from the spacecraft by the +4 to +5 V spacecraft potential.

The purpose of this paper is to report on the presence of just such a population, normally hidden by positive spacecraft potentials and revealed when the spacecraft enters eclipse and drops to near zero volts potential. Data from two spacecraft will be shown, Applied Technology Satellite 6 (ATS 6) and SCATHA (P78-2), using detectors designed at the University of California at San Diego (UCSD). These are described in the next section, followed by brief discussions of the normal charging behavior of the two satellites and of the normal relationship of the spacecraft orbits to the inner boundary of the plasma sheet. Four data sets follow, with the first ATS 6 spectrogram showing the appearance of the hidden ion population in the plasma sheet. The SCATHA examples which follow provide details of the spacecraft potential variations found in the plasma sheet when the spacecraft moves from sunlight into eclipse and finer energy resolution on examples of both the isotropic hidden ion population and the low-energy field-aligned population found near the plasma sheet boundary.

Spacecraft and Instruments

The data shown in this paper come from ATS 6 and the Air Force SCATHA satellite. ATS 6 was a three-axis-stabilized satellite in geosynchronous orbit, while SCATHA was spin-stabilized (tit rpm) in a nearly geosynchronous orbit, with a perigee of 5.5 RE and an apogee of 7.5 RE. The data shown here from SCATHA were taken at about 6 RE.

The UCSD particle detectors on these spacecraft were designed to measure the 1-eV to 80-keV plasma population. The ATS 6 instrument has been described in detail by Mauk and Mcllwain [1975], and only the main features are noted here. The electrostatic analyzers (ESA's) had an energy resolution (GE/E) of 20% and covered the 80-keV energy range in 64 steps in a 16-s period. Two pairs of ion and electron ESA's were mounted in rotating detector assemblies, with a fifth ion detector mounted to the spacecraft body. Data shown in this paper are from the north-south (NS) detector, which rotates through a $_{220}°$ range in 150 s, generally covering the 15°-155° pitch angle range with about 5° resolution.

The detector flown on SCATHA was modified so that three of the ESA's were limited to the 1-eV to 1800-eV energy range (one rotating assembly and the fixed ion detector). This and the elimination of noise problems in the plate voltages provide for greatly improved ion data in the 2- to 20-eV energy range. A frequently used command option was to suppress the low-energy (0-20 eV) electron data in order to increase the spiraltron lifetimes. Residual noise levels on the plates and variations in contact potentials combine to cause a sharp drop in efficiency below 1.8 eV. Pitch angle coverage was generally obtained by leaving the detectors fixed looking radially away from the satellite, and the 5°-175° pitch angle range was covered in 28 s as the spacecraft rotated. This period was badly matched to the 16-s energy scan period, and field-aligned measurements are made with some difficulty.

Paper number 2A0269. 0148-0227/82/002A-0269$05.00

A useful feature of the energy scan pattern is the ability to dwell at a few select energies for 2-28 s between energy scans. This can provide improved temporal or angular coverage at a few energies.

Spacecraft Potentials

Data from the UCSD detectors on ATS 5 and ATS 6 have been used to study spacecraft charging in both daylight and eclipse [DeForest, 1972; Olsen et al., 1981]. These studies have concentrated on the relatively large negative potentials (hundreds to thousands of volts) found in the midnight to dawn sector in hot plasma sheet environments. During quiet times, however, the spacecraft is normally a few volts positive in the midnight region. This is supported by analysis of ion engine operations on ATS 6 at quiet times which shifted the spacecraft from +5V to -4 V in sunlight [Olsen, 1981]. Positive potentials were inferred from breaks in the electron distribution functions, and negative potentials from ion charging peaks. This was a fairly unique data set because of both the ion engine operations and an unusual detector mode, which provided relatively high energy resolution. Quiet time eclipse data are consistent with a shift from about +10 V to +1 or +2 V, but a clear measurement of such a shift could not be made on ATS 6. The low-energy electron detector on SCATHA provides much better information on this shift. This shift will be illustrated in the first SCATHA example for a low-energy plasma sheet environment. The result is that the spacecraft falls from about +10 V to +1 to +3 V when it enters eclipse.

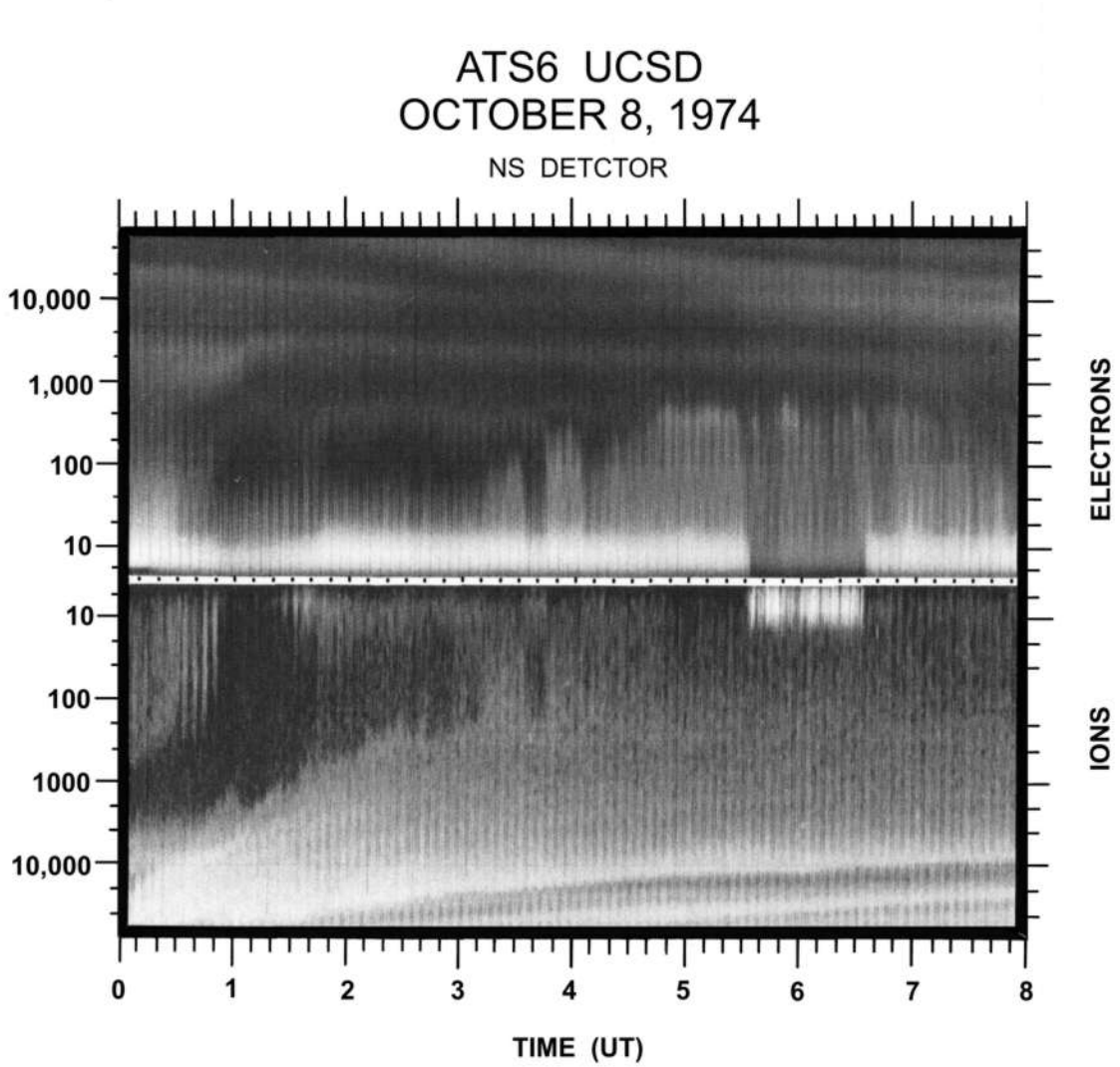

Fig. 1. Spectrogram for ATS 6 data, NS detector, October 8, 1974. Electron data are plotted in the top half of the figure, and ion data in the bottom half. Energy scales run vertically from 0 to 80 keV in logarithmic-fashion, with both scales starting from the center of the plot. The 8-hour tine scale runs horizontally. Count rates are plotted with a gray scale, black corresponding to low counts, and white to high count rates.

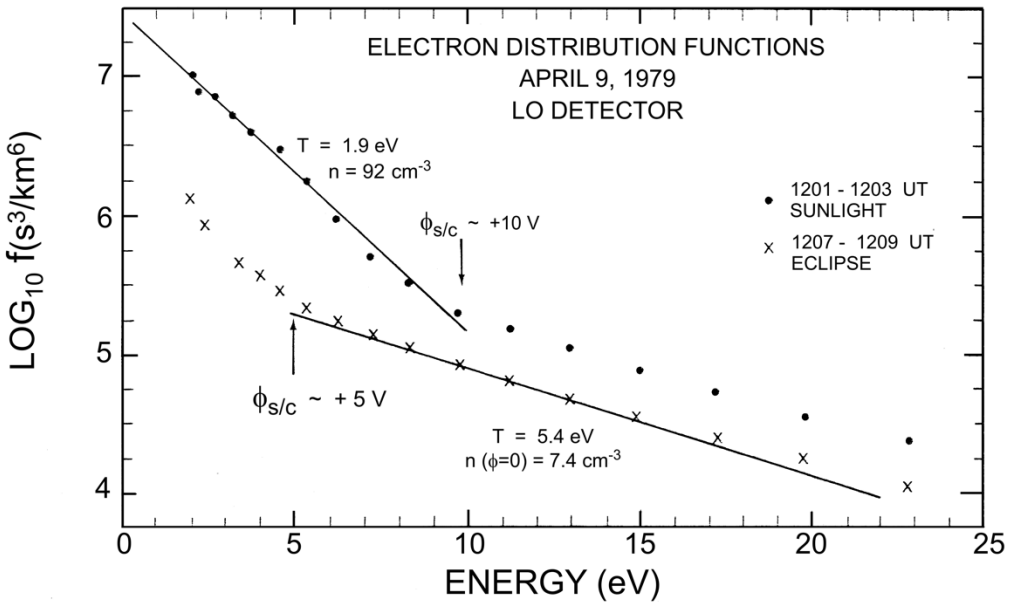

Fig. 2. Electron distribution functions, April 9, 1979. Data from the low-energy rotating detector in eclipse and sunlight show +5- and +10-V potentials, respectively.

The observation that the normal spacecraft potential in sunlight is several volts positive is not surprising, given the large photoelectron flux (of the order of 10 $\mu A/m^2$ [Grard, 1973]), the relatively low ambient electron density in the plasma sheet (~1-10 cm^{-3}), and the resulting low electron flux (0.1-1.0 $\mu A/m^2$). 'It might be expected that in eclipse the ambient electron flux would overwhelm the ambient ion flux, resulting in a spacecraft potential of the order of the electron energy. This indeed happens in high-energy environments [DeForest, 1972], but as the electron temperature drops below a few keV, secondary emission fluxes begin to exceed the ambient electron fluxes, resulting in a net positive current due to the ambient fluxes, and the spacecraft remains positive in eclipse.

Spacecraft Locations

One of the characteristics of geosynchronous orbit is that near local midnight the spacecraft is near the inner boundary of the plasma sheet during quiet times. This relationship between the spacecraft location and the plasma sheet boundary has been extensively explored as part of the study of magnetospheric convection patterns, particularly on the nightside. DeForest and McIlwain [1971], Mcllwain [1972], Eather et al. [1976], and Kivelson et al. [1979] have shown that the plasma sheet boundary observed by geosynchronous satellites corresponds to the zero-energy Alfven layer and that high-energy cutoffs in the electron data represent boundaries in space for plasma sheet convection at those energies. This approach to describing plasma sheet observations depends upon relatively static fields and a lack of substorm events near the spacecraft in space or time (i.e., no recent `instantaneous' injections). The cases presented in this paper all fall neatly into that category, showing little or no activity for several hours prior to the observations made at local midnight.

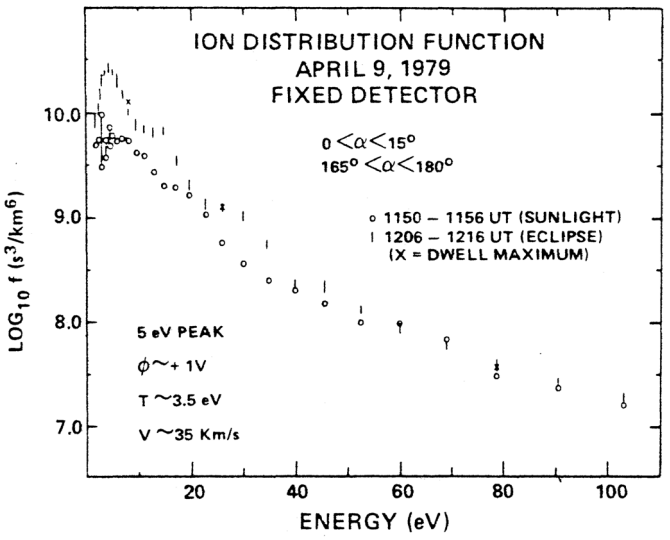

Fig. 3. Ion distribution functions, April 9, 1979. Field-aligned data from sunlight and eclipse verify the relative shift in spacecraft potential inferred from the electron data. The peak in the eclipse data probably represents a flow along the field line.

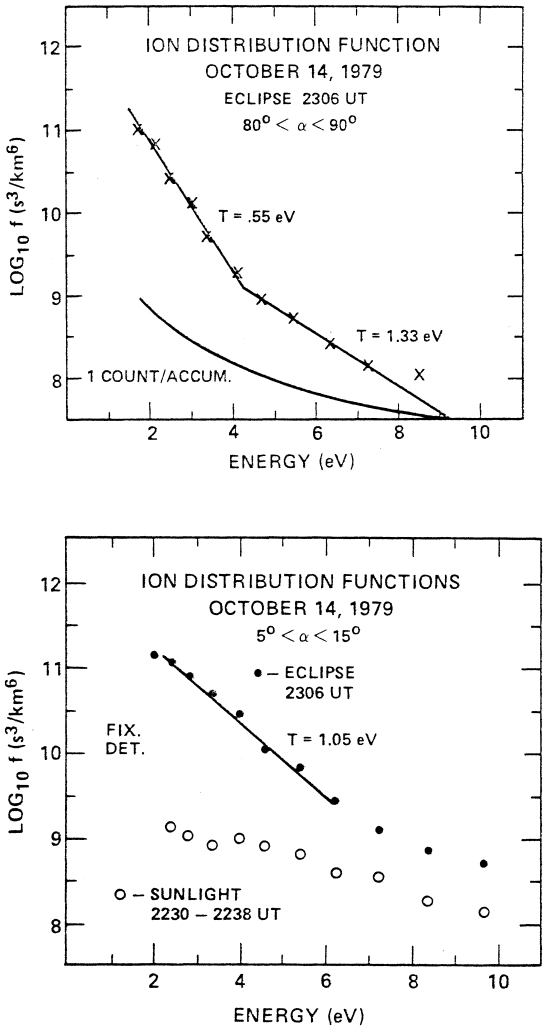

Fig. 4. Distribution functions from SCATHA ion detectors on October 14, 1979. (a) LO detector data perpendicular to $\vec{B}$ in eclipse. (b) FIX detector data parallel to $\vec{B}$ in eclipse and sunlight.

Observations

The first data set to be presented, from ATS 6, is intended to illustrate the appearance of the hidden ion population in a low-energy plasma sheet environment and to show that such measurements are not unique to one satellite. The examples from SCATHA which follow are intended to show the potentials found in and out of eclipse in such environments and to provide clearer looks at the hidden ion population distribution functions in and out of the plasma sheet.

ATS 6, October 8, 1974

The appearance of a thermal ion population in eclipse is illustrated in Figure 1, a spectrogram for 8 hours of data taken on October 8, 1974. The spacecraft entered the plasma sheet between 0300 and 0400 UT (2100-2200 LT), as indicated by the appearance of electrons in the 0- to 500-eV energy range. The convection pattern of the keV ions shows that this plasma sheet population had been focused at least several hours earlier. The appearance of 80-keV ions near 0000 UT (local dusk) implies that the last injection was at that time or earlier. The spacecraft is eclipsed by the earth at local midnight, from 0533 to 0632 UT as determined by the solar array telemetry. The ion count rate in the first few energy channels (2 and 5 eV) rises from background (less than 1 count/accumulation) to a relatively high flux of 100 counts/accumulation (400 cps). This flux is basically isotropic, as determined from the pitch angle sampling provided by the rotating detector, but does show somewhat higher fluxes parallel to the magnetic field line in the first half of the eclipse. The perpendicular component varies over the eclipse period, with the highest fluxes appearing in the latter half of the eclipse. The 0- to 20-eV electrons drop in intensity during the eclipse, reflecting the disappearance of the photoelectrons and the drop in spacecraft potential. The electron data are consistent with a drop from +10 V to +2 or +3 V. The ion data provide a lower limit of -2 V on the potential and are also consistent with a +2-V potential in eclipse. The relative lack of energy resolution for these distributions on ATS 6 is remedied with the SCATHA instrument, and analysis of the energy spectra will be postponed until those examples are presented.

This example is one of 42 eclipses encountered in the fall of 1974. During 23 of the eclipses the spacecraft charged hundreds to thousands of volts negative, as described by DeForest [1972] for ATS 5. The other 19 eclipses occurred at times where a lack of recent magnetic activity (substorms) resulted in environments with low temperatures (average energies). These low-temperature plasma sheet environments produced only the small shift in potential illustrated in Figure 1. This was the only one of the 19 events where a previously 'hidden' ion population appeared. The controlling factor appears to be a complete absence of recent magnetic activity (Kp = 1+ at this time) and a period of relative quiet over the previous day (October 7 had ΣKp = 12-). The singularity of the event makes it difficult to say more about the magnetic activity dependence of the thermal plasma.

SCATHA

Data from 89 eclipses in the spring and fall of 1979 from SCATHA show 39 cases of low potentials, and nine of these events revealed the existence of the hidden ion population. Unfortunately, the low-energy electron measurements were suppressed during the nine good events, and good measurements of the spacecraft potentials are not available. To resolve this lack, several of the cases of low eclipse potential (but no hidden ion population) were studied from the subset of events where the good electron measurements were available. These were all from low-energy plasma sheet populations, similar in all the events studied, so data from April 9, 1979, were chosen for presentation on the basis of the relatively clear ion data.

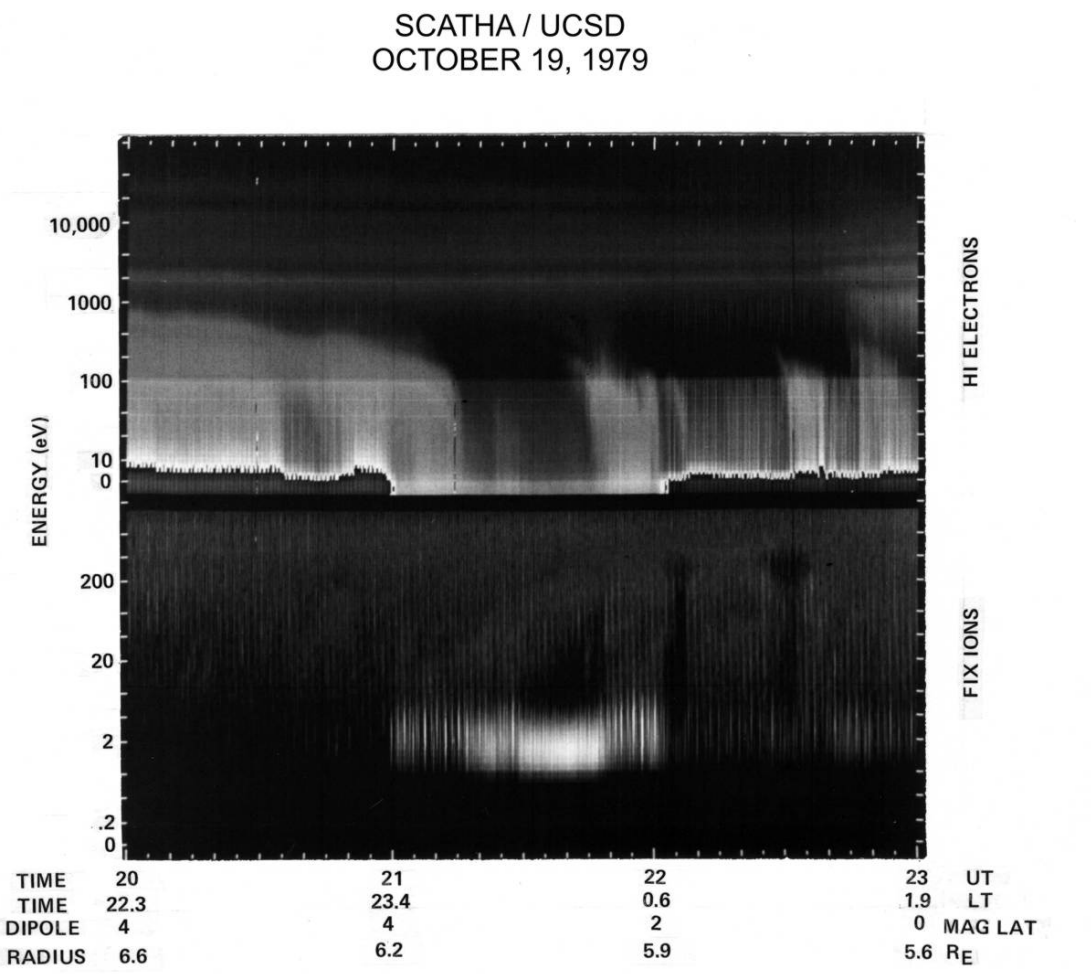

Fig. 5. Spectrogram for SCATHA FIX ion and HI electron data for 3 hours, centered at local midnight. The eclipse runs from 2100:30 to 2201:00 UT (from the solar array telemetry). The low-energy electron fluxes in sunlight (photoelectrons) are high enough to cause the gray scale to cycle back to black.

The hidden ion populations shown in the two examples which follow show an anisotropic distribution in an 'old' plasma sheet (formed at least 7-8 hours previously) and an extremely dense isotropic population which appears as the spacecraft drops out of the plasma sheet into the outer portion of the plasmasphere.

April 9, 1979

The electron data from April 9, 1979, in sunlight and eclipse are shown in Figure 2. The complementary ion data are shown in Figure 3. The electron distribution functions are taken at approximately 90° pitch angle, and at the same spacecraft attitude, in order to reduce pitch angle effects and effects due to spin modulation of the potential. The ion distributions were taken along the field line, since the perpendicular fluxes are suite low at this tire. The sunlight electron distribution function shows a clear bend at 10 eV, marking the boundary between the spacecraft-generated photoelectron and secondary electron population (E < 10 eV) and the ambient population. On some days, there is even a small electron 'charging peak,' a flux of cold electrons accelerated into one or two higher- energy channels, in analogy to the ion charging peak seen during large negative charging events. Also, on days when the ambient low-energy electron density is somewhat lower, there is occasionally a sharp drop of an order of magnitude in the distribution function at the (inferred) spacecraft potential.

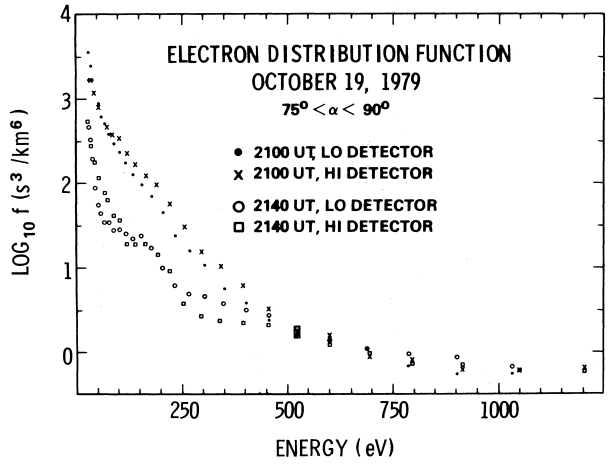

Fig. 6. Electron distribution functions, October 19, 1979. Trapped electron fluxes from two times in eclipse show the drop in 50- to 450-eV fluxes as the spacecraft crosses a plasma sheet boundary. Differences between the HI and LO detectors represent slight differences in look directions and detector calibrations.

The eclipse electron distribution function shows a bend at 5 eV, indicating that the potential has dropped to about +5 V. The two ambient distributions overlap when shifted by 5 eV, indicating that the potential has changed by that amount. The photoelectron population has a temperature of 1.9 eV, as determined by least squares fitting the 2.0- to 9.7-eV fluxes. The density for the photoelectrons, assuming they come from a source at the mainframe potential, is 92 cm^{-3}. (This gives ~12 $\mu A/m^2$ as the emitted flux.) The secondary electrons seen in eclipse (2.39-4.6 eV) show a temperature of 2.1 eV and a density of 8.5 cm^{-3}. The ambient population shows a temperature of 5.4-6.0 eV (eclipse and sunlight values, respectively) in the 2- to 10-eV ambient energy range and a density of 3.0 cm^{-3}), assuming potentials of +5 and +10 V in eclipse and sunlight, respectively. Note that the secondary flux in eclipse (~1.2 $\mu A/m^2$) is greater than the low-energy ambient flux (~0.7 $\mu A/m^2$)

The ion distribution functions shown in Figure 3 are considerably more complicated than the electron distributions but clearly show the 5-V shift. The field-aligned ion flux was visible in sunlight, with reasonably high count rates, but note that the 5-eV peak seen in eclipse is not seen in sunlight. Since the distribution is clearly non-Maxwellian, this peak cannot be inferred from a high-energy tail. One point of interest is that the ion distribution is clearly not field aligned above 10 eV or so, when dwell data provide clear pitch angle distributions. The 26- and 78-eV eclipse fluxes 2nd the 233-eV daylight flux all clearly peak at 10° and 12° away from the field line.

This data set has clearly shown the positive potentials found in sunlight and eclipse in a low-energy plasma sheet population (electron fluxes up to about 1 keV). One note of caution should be made, however, before the hidden ion events are presented. Since these events differ from the one just shown by the presence of a cold, isotropic ion population, it is reasonable to expect the presence of a cold ambient electron population. Such a population would cause the spacecraft potential to drop closer to zero in both sunlight and eclipse, conceivably to within a volt or so. The measurement of such a population is excluded by the same mode which prevents the measurement of photoelectrons.

October 14, 1979

Ion distribution functions from October 14, 1979 (day 287), are shown in Figures 4a and 4b. Figure 4a shows the perpendicular fluxes in eclipse, while Figure 4b shows the field-aligned fluxes in sunlight and eclipse. The spacecraft is in the plasma sheet, but it is again a relatively 'old' population. The high-energy ion fluxes show that the last injection of hot plasma was at least 7 hours before the eclipse, at 1600 UT or earlier. This is reflected in the electron data, which show a plasma sheet population ranging up to 17 keV but relatively low fluxes. The anisotropic pitch angle distribution is sampled simultaneously by the LO and FIX detectors, which are _looking along the spin axis (perpendicular to B) and radially (field aligned at this moment), respectively. The two detectors agree in their measurement of the perpendicular fluxes when the FIX detector comes around to the appropriate look direction, so the differences between the fluxes shown here are due only to pitch angle variations. The field-aligned fluxes (Figure 4b) are warmer than the perpendicular fluxes, as is usually the case, and there is a higher-energy tail to both populations. The hidden part of the perpendicular population is the 0.5-eV temperature portion of the plot (Figure 4a). Note that the tail of this distribution is again covered by the warmer population, and this population cannot be seen in sunlight. The field-aligned fluxes measured in daylight are considerably lower, as expected, but still measurable at about 10 counts/accumulation (30-40 cps at 3-4 eV). The sunlight distribution function is again shifted 4 or 5 eV from the eclipse distribution, indicating the shift in potential between the two times.

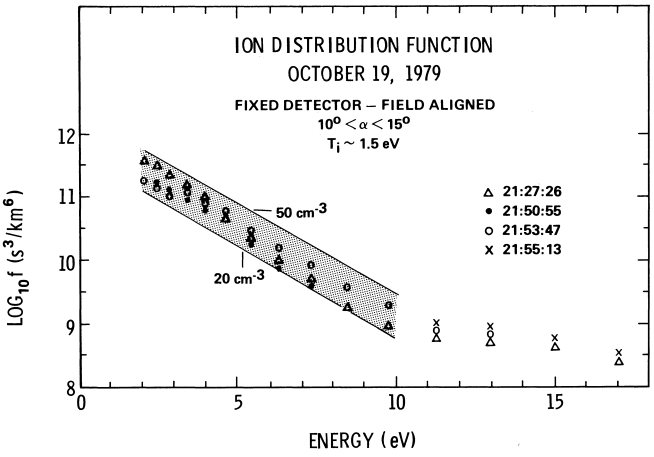

Fig. 7. Ion distribution functions, October 19, 1979. Field-aligned fluxes are shown for several times during eclipse. The data are bounded by a 1.5-eV Maxwellian distribution with a density between 20 and 50 cm^{-3}.

The distribution functions were least squares fitted assuming an isotropic Maxwellian distribution, resulting in temperature and density estimates for both field-aligned and perpendicular fluxes. The density is not a true density but rather the result of calculating the intercept of the fit with the vertical axis for a small portion of the distribution function. This parameter, a pseudodensity, is designated $4\pi\partial n/\partial\Omega$ In an isotropic, single-temperature, Maxwellian environment, it would be the actual density, uncorrected for spacecraft potential. The value obtained for the perpendicular, 0.55 eV component was 13 cm^{-3}, with the higher energy perpendicular flux (T = 1.33 eV) giving $4\pi\partial n/\partial\Omega$ = 0.7 cm^{-3}. The 1-eV field-aligned flux gave a value of 17 cm^{-3}.

October 19, 1979

Data from October 19, 1979, are shown in Figures 5-8. Figure 5 is a spectrogram for the ion data from the FIX detector and the electron data from the HI detector. The eclipse period (2100-2200) is signaled by the disappearance of the photoelectrons and the intensification of the low-energy ion fluxes. The high-energy fluxes (not shown) indicate that no injections of hot plasma have occurred on these drift shells in the previous 10-20 hours. This is reflected in the limited energy range of the plasma sheet electrons seen in Figure 5. The cutoff in flux starts at 1 keV at 2000 UT and drops steadily in energy with time. At the beginning of the eclipse the cutoff is at a few hundred eV, and by 2120 UT this population has disappeared. The spacecraft is moving radially inward at this time and appears to have dropped out of the plasma sheet. The electron distribution functions shown in Figure 6 show that at 2100 UT, at the beginning of the eclipse, there is a bend in the curve at 400 eV, signaling a transition from one population to another. The 0- to 400-eV population (T ~ 75 eV) has disappeared by 2140, and only a low flux of a different, perhaps older, population remains. The constancy of the distribution function above 400 eV suggests that any spatial boundary for this population must be further inward.

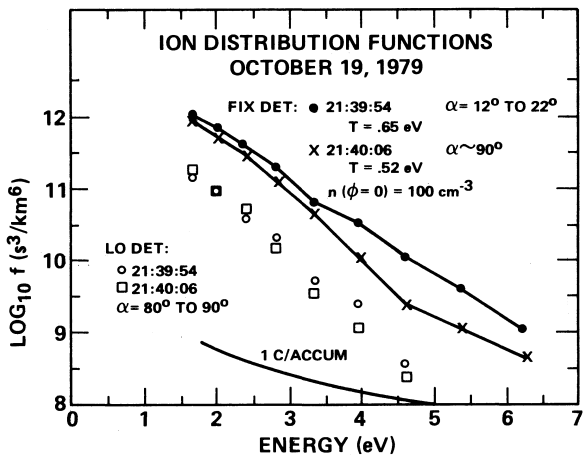

Fig. 8. Ion distribution functions from SCATHA FIX and LO detectors on October 19, 1979, for field-aligned and perpendicular fluxes.

The ion fluxes seen in the spectrogram show the vertical striping signature of a pitch angle distribution early in the eclipse, in the plasma sheet. As the electron flux disappears, a solid white region (2120-2150) indicates an isotropic region. This is followed by a return to the plasma sheet and anisotropic fluxes (2150-2200). The dark region below 1.8 eV in the ion data shows the sharp drop in detector efficiency at that energy. The field-aligned ion data are reasonably constant throughout the eclipse period, as shown in Figure 7. The distribution functions measured in eclipse are acquired in a few seconds, while the spacecraft has rotated several degrees, and some of the variations in the distribution functions may be due to variations in pitch angle over the energy scan period. With this proviso, it appears that the 1- to 10-eV field-aligned ion population is well characterized as a 1.5-eV, 20- to 50-cm^{-3} population, with a higher-energy tail. (This is again the fitted density. Since the field-aligned distribution fills about 10% of the solid angle, divide by 10 for an estimate of the contribution to the total density.)

The cold, dense, isotropic ion population which appears when the spacecraft drops out of the plasma sheet is shown in Figure 8. Data from both the low-energy ion detectors are shown here to demonstrate the isotropic nature of the new environment. On this day, at the spiraltron bias levels in use, the low-energy rotating detector (LO) shows substantial degradation in the ion channel. Data from this channel are therefore shown only to emphasize that the environment is constant over the 10 to 15 s required to make the perpendicular and parallel measurements with the fixed detector. The 0.5-eV ion population is clearly isotropic over the 1.6- to 3.3-eV energy range, with the field-aligned fluxes rising above the perpendicular fluxes above 4 eV, with a higher temperature (1.5 eV as just shown in Figure 7). The fitted density for the isotropic population is between 100 and 150 cm^{-3} during the 10-min period the spacecraft spent inside the plasma sheet boundary. The spacecraft potential must be at or below the +5-V potential seen in thinner plasma environments but cannot be more than 1.5 V negative, by the evidence of the ion data. If the spacecraft is as much as 2 V positive, the isotropic plasma shown here would have a density of thousands per cubic centimeter, and there would be a complementary electron population which would be visible in the high-energy detector, if poorly resolved. No such fluxes are apparent in that detector, and it seems reasonable to set an upper bound of +1 V on the spacecraft potential and an upper bound of 500 cm^{-3} on the density. A lower limit of -1 V provides a lower bound on the density of 20 cm^{-3}, an unusually high value for the plasma density at 6.0 R_E.

Discussion

A cold, dense, isotropic ion population has been shown to exist near the inner edge of the plasma sheet at local midnight between 6.0 and 6.6 R_E. The 1-eV population is typically hidden by a spacecraft potential of +5 to +10 V. During eclipses of the spacecraft, a drop in the photoelectric current allows the potential to drop by 5 or 6 V, and the cold ion population can be measured. The hidden ion population is found at geosynchronous altitude only at quiet times, i.e., when Kp is 2 or less, and when there has been an absence of magnetic activity (from the L = 6 perspective) for several hours.

The cold plasma appears to coexist with the plasma sheet, penetrating into the 400- to 500-eV Alfven layer. This is important for most wave-particle interaction processes, where the presence or absence of a cold plasma can deter-mine whether or not waves will grow or be damped.

Viewing the cold ion population at other local times, or more controllably at midnight, will require a method of biasing the ion detector with respect to the spacecraft or of controlling the potential of the entire spacecraft. The former method has been employed with a thermal plasma detector on GEOS 1 and 2 with some success [Johnson et al., 1978]. The detector is extended on a boom, and the entire package is biased with respect to the mainframe of the satellite. This method appears to work fairly well but leaves substantial questions about the effects of the electrostatic and space charge distributions around the satellite on the particle measurements. During the deployment of the 50-m electric field antenna on SCATHA, it was noted that there was a local minimum in the probe potential of a volt or so several meters away from the satellite (T. Aggson, private communication, 1981). A boom-mounted particle detector should be mounted a substantial distance from the mainframe if sheath effects are to be avoided.

The alternative of biasing the spacecraft potential has been addressed by Olsen [1981]. Plasma emission experiments with the ion engine on ATS 6 showed the feasibility of using plasma emission to bias the normally positive spacecraft slightly negative, greatly enhancing the low-energy ion measurements. Practical application of such a technique requires mass analysis of the low-energy ions to reject the artificially generated plasma, but does not appear to have other significant problems. Emission of a plasma also serves to eliminate large negative potentials and tends to make the spacecraft surface more of an isopotential, so this technique could prove valuable for several reasons.

Acknowledgements. This work was supported by NASA contract NAS5-23481, and NASA grant NSG-3150 while at the University of California at San Diego, and the SCATHA data were analyzed under Air Force contract F04701-77C-0062. Further work was supported by NASA contract NAS-8-33982 at the University of Alabama in Huntsville. The author would like to thank C. E. Mcllwain for providing the ATS 6 data and S. E. DeForest for the SCATHA data. B. Ledley provided the SCATHA magnetic field data needed for pitch angle calculation.

The Editor thanks B. H. Mauk and D. Winningham for their assistance in evaluating this paper.

References

Decreau, P. M. E., J. Etcheto, K. Knott, A. Pedersen, G. L. Wrenn, and D. T. Young, Multiexperiment determination of plasma density and temperature, *Space Sci. Rev.*, 22, 633-645, 1978.

DeForest, S. E.., Spacecraft charging at synchronous orbit, *J. Geophys. Res.*, 77, 651-659, 1972.

DeForest, S. E., and C. E. Mcllwain, Plasma clouds in the magnetosphere, *J. Geophys. Res.,* 76, 3587-3610, 1971.

Eather, R. H., S. B. Mende, and R. J. R. Judge, Plasma injection at synchronous orbit and spatial and temporal auroral morphology, *J. Geophys. Res.,* 81, 2805-2824, 1976.

Grard, R. J. L., Properties of the satellite photoelectron sheath derived from photoemission laboratory measurements, *J. Geophys. Res.,* 78, 2885-2906, 1973.

Gurnett, D. A., and L. A. Frank, Thermal and suprathermal plasma densities in the outer magnetosphere, *J. Geophys. Res.*, 79, 2355-2361, 1974.

Johnson, J. F. E., J. J. Sojka, and G. L. Wrenn, Thermal/suprathermal plasmas observed by the S-302 experiment on GEOS-1, *Space Sci. Rev.*, 22, 567-580, 1978.

Kivelson, M. G., S. M. Kaye, and D. J. Southwood, The physics of plasma injection events, in *Dynamics of the Magnetosphere,* edited by S.-I. Akasofu, pp. 385-405, D. Reidel, Hingham, Mass., 1979.

Mauk, B. H., and C. E. Mcllwain, ATS 6 UCSD auroral particles experiment, *IEEE Trans. Aerosp. Electron. Syst., AES-11,* 1125-1130, 1975.

Mcllwain, C. E., Plasma convection in the vicinity of the geosynchronous orbit, in *Earth's Magnetospheric Processes,* edited by B. M. McCormac, pp. 268-279, D. Reidel, Hingham, Mass., 1972.

Olsen, R. C., Modification of spacecraft potentials by plasma emission, *J. Spacecr. Rockets*, 18, 462-469, 1981.

Olsen, R. C., C. E. Mcllwain, and E. C. Whipple, Observations of differential charging effects on ATS 6, *J. Geophys. Res.*, 86, 6809-6819, 1981.

(Received October 19, 1981;
revised February 11, 1982;
accepted February 9, 1982.)